AD-A172 112 ULTRASONIC CHARACTERIZATION OF MATERIAL PROPERTIES OF COMPOSITE MATERIALS(U) COLORADO UNIV AT BOULDER DEPT OF MECHANICAL ENGINEERING S K DATTA ET AL. JUL 86 1/1

UNCLASSIFIED CUMER-86-1 N00014-86-K-0280 F/G 11/4 NL

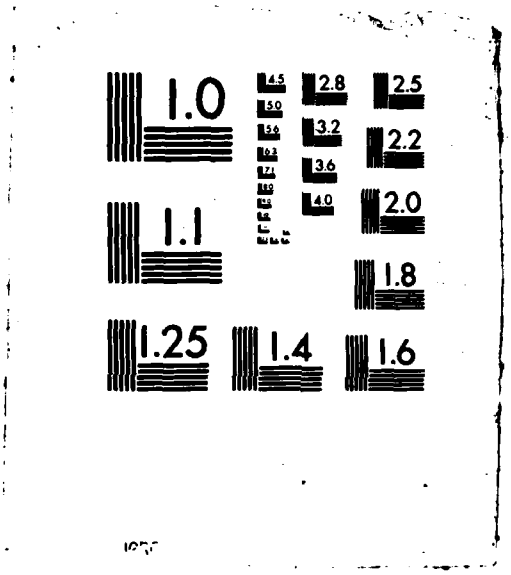
1.0
1.1
1.25
1.4
1.6
1.8
2.0
2.2
2.5
2.8
3.2
3.6
4.0
4.5
5.0
5.6

UNIVERSITY OF COLORADO

Ultrasonic Characterization of
Material Properties of Composite Materials

S.K. Datta
Department of Mechanical Engineering and CIRES
University of Colorado, Boulder, CO 80309

H.M. Ledbetter
Fracture and Deformation Division
National Bureau of Standards, Boulder, CO 8030

CUMER 86-1 July, 198

DEPARTMENT OF
MECHANICAL ENGINEERING

College of Engineering
Boulder, Colorado

Ultrasonic Characterization of Material Properties of Composite Materials

S.K. Datta
Department of Mechanical Engineering and CIRES
University of Colorado, Boulder, CO 80309

H.M. Ledbetter
Fracture and Deformation Division
National Bureau of Standards, Boulder, CO 80303

CUMER 86-1 July, 1986

Office of Naval Research Contract N00014-86-K-0280

ABSTRACT

Ultrasonic waves provide an excellent means to study the mechanical properties of both heterogeneous and composite materials. Recently, both theoretically and experimentally, we studied characteristics of elastic wave propagation through fiber and particle reinforced composites. Theoretically we analyzed phase velocities of longitudinal and shear waves propagating through composite media with aligned continuous fibers and ellipsoidal shaped particles. Alignment of reinforcing fibers (or particles) imparts anisotropy to the effective mechanical and physical properties of the composite. Theoretically, we modeled the anisotropic phase velocities, which agree with experimental measurements. One important feature of this combined theoretical and experimental study is the possibility of obtaining the (often uncertain) fiber (or particle) elastic properties by comparing the model predictions with the observations.

We show that one can use the theoretical model to obtain effective properties of media containing voids (pores). As examples, we consider porous olivine and creep cavities in copper. In the latter case some experimental results are presented which show good agreement with predictions.

Finally, we present some results for attenuation in a particulate composite including the effect of non-ideal interface properties.

INTRODUCTION

Determination of effective elastic moduli and damping properties of a heterogeneous material by using elastic waves (propagating or standing) is very effective. Several theoretical studies show that for long wavelengths one can calculate the effective wave speeds of plane longitudinal and shear waves through a composite material. At long wavelengths the wave speeds thus calculated are non-dispersive and hence provide the values for the static effective elastic properties. References to some of the recent theoretical and experimental works can be found in (1-13). The scattering formulations developed in (1-8) provide a means to obtain not only the effective wave speeds but also the damping of wave amplitudes due to scattering.

In this paper we present results of some of our recent investigations of phase velocity and attenuation of plane longitudinal and shear waves propagating in a medium with microstructure. Microstructures studied were either inclusions or fibers. In the former case, we examined the effect of inclusion shape, orientation, volume fraction, and elastic properties on wave speeds. For fiber-reinforced materials we studied continuous aligned fibers. In either case the medium behaves anisotropically because of the alignment of the inclusions or the fibers.

The theoretical model used a wave-scattering approach together with Lax's quasi-crystalline approximation and predicted the macroscopic isotropic elastic properties for the case of random orientation of inclusions and anisotropic elastic properties caused by preferred orientation. Both homogeneous and non-homogeneous distributions of inclusions or fibers were considered. The scattering approach led also to an estimation of attenuation via the use of optical theorem.

The experimental methods consisted of a pulse-echo technique and the resonance method. These were chosen to provide the advantages of small specimens and low inaccuracy. For details of the experimental techniques the reader is referred to (10-14,15).

Both homogeneous and nonhomogeneous distributions of inclusions and fibers were considered. First, we examined the case of a random homogeneous distribution of randomly oriented spheroidal inclusions in a homogeneous matrix. Second, we considered a random homogeneous distribution of oriented spheroids. In the first case the macroscopic properties of the composite are isotropic. In the second aligned spheroidal inclusions impart anisotropy to the composite. In order to model the SiC-particle-reinforced composite shown in Fig. 1 we used a two-step process combining the two distributions described above. In this example the material consists of "islands" of oriented oblate spheroidal Al inclusions in a "sea" of randomly oriented SiC prolate spheroidal inclusions. We also examined by the two-step process mentioned above the fiber-reinforced composite shown in Fig. 2 which consists of a nonhomogeneous distribution of aligned continuous

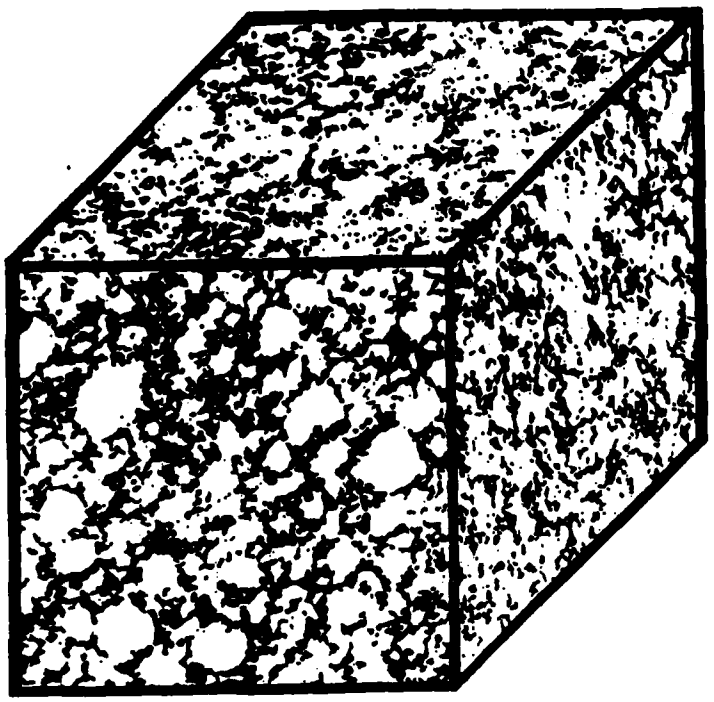

100 μm

Fig. 1 Photomicrograph of SiC/Al-alloy composite formed from powders of SiC and Al alloy. For present purposes we represent the SiC particles as prolate ellipsoids with an aspect ratio of 3.0. We represent the large Al "islands" as oblate spheroids (aligned in the rolling plane) with an aspect ratio of 0.33. The randomly oriented SiC particles exist in a "sea" where the SiC volume fraction is approximately double that of the macroscopic average volume fraction. The SiC particles range up to 5 μm in their largest dimension. The Al "island" particles range up to 60 μm.

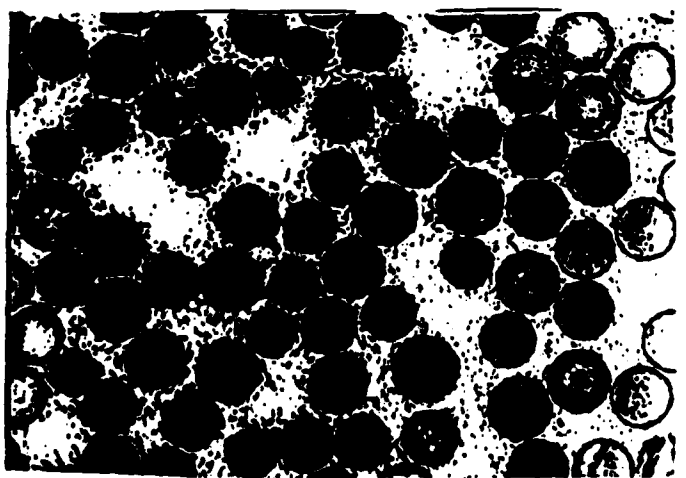

Fig. 2. Photomicrograph of Al_2O_3/Al alloy composite. Uniaxial Al_2O_3 fibers are 20 ± 5 μm in diameter. Note nonhomogeneous fiber distribution.

Al_2O_3 fibers in Al matrix.

In the following we describe the theoretical technique first in connection with a composite consisting of ellipsoidal shaped inclusions in a homogeneous matrix. Specialization to the two-dimensional case of fiber-reinforced materials is then briefly discussed. Model predictions are then compared with experimental results. Finally, we present some model calculations for attenuation in a particle-reinforced composite and for elastic properties of materials with voids.

MULTIPLE SCATTERING BY A DISTRIBUTION OF ELLIPSOIDAL INCLUSIONS

In this section the scattered field at any point in the matrix is obtained in the presence of a distribution of N ellipsoidal inclusions. We consider both aligned and nonaligned cases. The results obtained are valid when the wavelength is long compared to the inclusion dimensions. The method represents an extension to the elastic case of the approach used in (16, 17).

In expressing the scattered field in the presence of a number of ellipsoidal inclusions we must recall the results for a single ellipsoidal inclusion (18). Let the center of the i-th ellipsoid be located at (X_i, Y_i, Z_i) referred to a Cartesian frame of reference axes; let the principal axes of this ellipsoid be obtained from the Cartesian axes (XYZ) by rotation defined by the Eulerian angles α_i, β_i, γ_i. Let $\underline{u}^E(R|\rho_i)$ denote the total field incident on the i-th inclusion. In terms of vector spherical wave functions that are regular at ρ_i, this "exciting" field may be written quite generally as

$$\underline{u}^E(R|\rho_i) = \sum_{n=0}^{2} \sum_{m=-n}^{n} [a_{imn} L_{imn}^{(1)}(r_i,\theta_i,\phi_i) + \tau b_{imn} N_{imn}^{(1)}(r_i,\theta_i,\phi_i) + \tau c_{imn} M_{imn}^{(1)}(r_i,\theta_i,\phi_i)] \quad (1)$$

where r_i, θ_i, ϕ_i are the spherical polar coordinates of the point P with

$$r_i = [(X - \xi_i)^2 + (Y - \eta_i)^2 + (Z - \zeta_i)^2]^{1/2}$$

$$Z - \zeta_i = r_i\cos\theta_i, \quad X - \xi_i = r_i\sin\theta_i\cos\phi_i,$$

$$Y - \eta_i = r_i\sin\theta_i\sin\phi_i \quad (2)$$

position vector R referred to the center of the ellipsoid. Thus, in writing Eq. (1) we assume that the time dependence is through the factor $e^{-i\omega t}$, which has been dropped. The vector wave functions appearing in Eq. (1) were given in (18). τ is the ratio of the longitudinal-wave and shear-wave speeds in the matrix. The field given by Eq. (1) will be scattered by the ellipsoid and this scattered field, denoted by

$$\underline{u}^S(R|\rho_i) = \sum_{\nu=0}^{2} \sum_{\mu=-\nu}^{\nu} [A_{i\mu\nu} L_{i\mu\nu}^{(3)}(r_i,\theta_i,\phi_i) + \tau B_{i\mu\nu} N_{i\mu\nu}^{(3)}(r_i,\theta_i,\phi_i)] \quad (3)$$

where $L_{i\mu\nu}^{(3)}$ and $N_{i\mu\nu}^{(3)}$ are the appropriate spherical vector wave functions that satisfy the radiation conditions as $r_i \to \infty$. Here $\epsilon = \omega c/c_1$, where c_1 denotes the

longitudinal wave speed in the matrix and the principal semiaxes of the ellipsoid are a,b,c(a>b>c). Equations (1) and (3) keep terms to $O(\epsilon^3)$.

The relationships between the scattered-field coefficients $A_{i\mu\nu}$, $B_{i\mu\nu}$ and the incident-field coefficients a_{imn}, b_{imn}, and c_{imn} were derived in (18) when the semiaxes of the ellipsoid were parallel to the Cartesian axes XYZ. For aligned ellipsoids this choice can be made without loss of generality. However, for a nonaligned configuration it is necessary to obtain these relationships for arbitrary orientation. To derive these general relations from the results of (18) it is necessary to refer both the incident field (1) and the scattered field (2) to the ellipsoid axes. This is done by using the rotational addition theorems for spherical harmonics (19,20). One can show that

$$\underline{u}^E(R|R_i) = \sum_{n=0}^{2} \sum_{m'=-n}^{n} [a_{im'n} \underline{L}^{(1)}_{im'n}(r_i,\theta_i',\phi_i') + \tau b_{im'n} \underline{N}^{(1)}_{im'n}(r_i,\theta_i',\phi_i') + \tau c_{im'n} \underline{M}^{(1)}_{im'n}(r_i,\theta_i',\phi_i')] \quad (4)$$

In writing Eq. (4) the relations expressing the spherical vector wave functions referred to XYZ and the ellipsoidal axes have been used. These have the form:

$$\underline{L}^{(1)}_{imn}(r,\theta,\phi) = \sum_{m'=-n}^{n} B(m,m',n)\, \underline{L}_{im'n}(r,\theta',\phi') \quad (5)$$

Similar expressions hold for $\underline{M}^{(1)}_{imn}$ and $\underline{N}^{(1)}_{imn}$. Here

$$B(m,m',n) = (-1)^{m+m'} \left[\frac{(n+m)!(n-m')!}{(n-m)!(n+m')!}\right]^{1/2} D^{(n)}_{m'm}(\alpha\beta\gamma) \quad (6)$$

Using Eq. (5) in Eq. (1) it follows that

$$a_{im'n} = \sum_{m=-n}^{n} a_{imn}\, B(m,m',n), \text{ etc.} \quad (7)$$

The scattered field referred to the new axes is then

$$\underline{u}^S(R|R_i) = \sum_{\nu=0}^{2} \sum_{\mu'=-\nu}^{\nu} [A_{i\mu'\nu} \underline{L}^{(3)}_{i\mu'\nu}(r,\theta',\phi') + \tau B_{i\mu'\nu} \underline{N}^{(3)}_{i\mu'\nu}(r,\theta',\phi')] \quad (8)$$

Now

$$\underline{L}^{(3)}_{i\mu'\nu}(r,\theta',\phi') = \sum_{\mu=-\nu}^{\nu} \bar{B}(\mu',\mu,\nu)\, \underline{L}^{(3)}_{i\mu\nu}(r,\theta,\phi)$$

where

$$\bar{B}(m',\mu,n) = (-1)^{m'+\mu} \left[\frac{(n+m')!(n-\mu)!}{(n-m')!(n+\mu)!}\right]^{1/2} D^{(n)*}_{m'\mu}(\alpha\beta\gamma) \quad (9)$$

and the asterisk denotes complex conjugate. Thus,

$$A_{i\mu\nu} = \sum_{\mu'=-\nu}^{\nu} \bar{B}(\mu',\mu,\nu)\, A_{i\mu'\nu}$$

$$B_{i\mu\nu} = \sum_{\mu'} \bar{B}(\mu',\mu,\nu) B_{i\mu'\nu} \quad (10)$$

But

$$A_{i\mu'\nu} = \frac{iv_0\epsilon^3}{4\pi c^3} \sum_{\nu_1} \sum_{\mu_1}^{\mu_1\nu_1} T_{\mu'\nu}\, (a_{i\mu_1\nu_1} + \delta(\nu) b_{i\mu_1\nu_1}) \quad (11)$$

where

$$\delta(\nu) = 3\tau^2, \quad \nu = 0,2$$

$$= 2\tau, \quad \nu = 1$$

Explicit expressions for $T^{\mu_1\nu_1}_{\mu\nu}$ are given in (9).

Using Eqs. (7) and (11) in Eq. (10) it is found that

$$A_{i\mu\nu} = \frac{iv_0\epsilon^3}{4\pi c^3} \sum_{\nu_1} \sum_{\mu_1} \tilde{T}^{\mu_1\nu_1}_{\mu\nu} (a_{i\mu_1'\nu_1} + \delta(\nu)\, b_{i\mu_1'\nu_1})$$

$$B_{i\mu\nu} = \frac{iv_0\epsilon^3}{4\pi c^3} \Delta(\nu) \sum_{\nu_1} \sum_{\mu_1} \tilde{T}^{\mu_1'\nu_1}_{\mu\nu} (a_{i\mu_1'\nu_1} + \delta(\nu)\, b_{i\mu_1'\nu_1}) \quad (12)$$

where

$$\tilde{T}^{\mu_1'\nu_1}_{\mu\nu} = \sum_{\mu'=-\nu}^{\nu} \sum_{\mu_1=-\nu_1}^{\nu_1} \bar{B}(\mu',\mu,\nu)\, T^{\mu_1\nu_1}_{\mu'\nu}\, B(\mu_1',\mu_1,\nu_1)$$

$$\Delta(\nu) = \begin{cases} \tau^2, & \nu = 1 \\ \tau^3/2, & \nu = 0, 2 \end{cases}$$

This completes the derivation of the scattered field due to a single arbitrarily oriented ellipsoid.

We now seek the scattered field due to a number of arbitrarily oriented ellipsoids. It is necessary to expand the scattered field due to the j-th ellipsoid in vector wave functions regular near the i-th one. Using translational addition theorems (21) the exciting field on the i-th ellipsoid is

$$\underline{u}^E(R|R_i) = \underline{u}^{(i)} + \sum_{n=0}^{2} \sum_{m=-n}^{n} [a^2_{imn} \underline{L}^{(1)}_{imn} + \tau b^2_{imn} \underline{N}^{(1)}_{imn} + \tau c^2_{imn} \underline{M}^{(1)}_{imn}] \quad (13)$$

where

$$a^2_{imn} = \sum_{j\neq i} \sum_{\nu} \sum_{\mu'=-\nu}^{\nu} A_{j\mu'\nu} A^{\mu'\nu}_{mn}$$

$$b^2_{imn} = \sum_{j\neq i} \sum_{\nu} \sum_{\mu'=-\nu}^{\nu} B_{j\mu'\nu} B^{\mu'\nu}_{mn}$$

Here $\underline{u}^{(i)}$ is the incident field and $A^{\mu'\nu}_{mn}$ and $B^{\mu\nu}_{mn}$ are defined in (2).

The incident wave will be taken as a plane wave propagating along the Z-axis. Thus, it may be written as

$$\underline{u}^{(i)} = \underline{e}_z\, e^{ik_1 Z} + \underline{e}_x\, e^{ik_2 Z}$$

$$= \frac{e^{ik_1\zeta_i}}{i} \sum_{n=0}^{\infty} \sum_{m} i^n(2n+1)\, \underset{\sim}{L}^{(1)}_{imn}\, \delta_{m0} +$$

$$+ \frac{1}{2i} e^{ik_2\zeta_i} \sum_{n=1} \sum_{m} \frac{2n+1}{n(n+1)}\, i^n \left(\underset{\sim}{M}^{(1)}_{imn} (\delta_{m1} + n(n+1)\, \delta_{m,-1}) + \underset{\sim}{N}^{(1)}_{imn} (\delta_{m1} - n(n+1)\delta_{m,-1})\right) \qquad (14)$$

So

$$a_{imn} = \frac{e^{ik_1\zeta_i}}{i}\, i^n(2n+1)\, \delta_{m0} + \sum_{j\neq i} \sum_{\nu} \sum_{\mu'} A_{j\mu'\nu}\, A^{\mu'\nu}_{mn} \qquad (15)$$

$$b_{imn} = \frac{e^{ik_2\zeta_i}}{i}\, \frac{i^n(2n+1)}{2n(n+1)} [\delta_{m1} - n(n+1)\, \delta_{m,-1}] + \sum_{j\neq i} \sum_{\nu} \sum_{\mu'} B_{j\mu'\nu}\, B^{\mu'\nu}_{mn} \qquad (16)$$

Using Eqs. (15) and (16) in Eq. (12) the scattered-field coefficients correct to $O(\epsilon^3)$ due to a number of arbitrarily oriented ellipsoids are obtained. In this study the calculations are simplified if we assume that the distribution of particles is random and homogeneous. We assume further that the particles have the same shape and size.

Frequently, the processing of these composites produces a material that contains nonhomogeneities, for example matrix islands devoid of particles (see Fig. 1). This fact is considered in a second-step calculation that assumes that there is a distribution of aligned oblate-spheroidal matrix-material inclusions in the composite.

EFFECTIVE WAVE SPEEDS IN A COMPOSITE OF RANDOM DISTRIBUTION OF DISORIENTED ELLIPSOIDS

To calculate the effective wave speeds of plane waves, we take an ensemble average of Eq. (12). For this purpose, the probability density of finding the scatterers at $\underset{\sim}{R}_1$, $\underset{\sim}{R}_2$, ... is denoted by $p(\underset{\sim}{R}_1,\ldots,\underset{\sim}{R}_N)$, which can be written

$$p(\underset{\sim}{R}_1,\ldots,\underset{\sim}{R}_N) = p(\underset{\sim}{R}_1)\, p(\underset{\sim}{R}_2,\ldots,\underset{\sim}{R}_N|\underset{\sim}{R}_1)$$

$$= p(\underset{\sim}{R}_1)\, p(\underset{\sim}{R}_2|\underset{\sim}{R}_1)\, p(\underset{\sim}{R}_3,\ldots,\underset{\sim}{R}_N|\underset{\sim}{R}_1,\underset{\sim}{R}_2) \qquad (17)$$

Assuming the distribution to be uniform it follows that

$$p(\underset{\sim}{R}_1) = 1/V\ ,\ \underset{\sim}{R}_1 \in V$$

$$= 0\ ,\ \underset{\sim}{R}_1 \notin V \qquad (18)$$

where V is the volume of the composite. Furthermore, following the analyses of (3), the conditional density $p(\underset{\sim}{R}_2|\underset{\sim}{R}_1)$ will be taken

$$p(\underset{\sim}{R}_2|\underset{\sim}{R}_1) = 1/V\ ,\ |\underset{\sim}{R}_2 - \underset{\sim}{R}_1| \geq 2a$$

$$= 0\ ,\ |\underset{\sim}{R}_2 - \underset{\sim}{R}_1| < 2a \qquad (19)$$

This is the "well-stirred" approximation whose validity for high concentrations is open to question (7). However, the results obtained in (2) under this assumption coincide with the lower (upper) bound of Hashin and Shtrikman (22). (See Ref. (3).) Although this is no justification for adopting Eq. (19), we use it here for simplicity.

In taking the ensemble average of Eq. (12), for random orientation, the average of $T^{\mu_i'\nu_1}_{\mu\nu}$ over all orientations is simply

$$\langle T^{\mu_1'\nu_1}_{\mu\nu} \rangle = 3\, P_\nu = \sum_{\mu_1=-\nu}^{\nu} \frac{1}{2\nu+1}\, T^{\mu_1\nu}_{\mu_1\nu} \qquad (20)$$

Thus,

$$\langle A_{i\mu\nu} \rangle_i = \frac{iv_0c^3}{4\pi C^3}\, 3\, P_\nu \left[\frac{1}{i} e^{ik_1\zeta_i}\, i^\nu(2\nu+1)\, \delta_{\mu 0} + n_0 \sum_{\nu_1}\sum_{\mu_1} \int_{|\underset{\sim}{R}_j - \underset{\sim}{R}_i| \geq 2a} \langle A_{j\mu_1\nu_1} \rangle_{ji}\, A^{\mu_1\nu_1}_{\mu\nu}\, d\underset{\sim}{R}_j + \delta(\nu)\left(\frac{1}{i} e^{ik_2\zeta_i}\, i^\nu\, \frac{2\nu+1}{2\nu(\nu+1)} (\delta_{\mu 1} - \nu(\ \ 1)\delta_{\mu,-1}) + n_0 \sum_{\nu_1}\sum_{\mu_1} \Delta(\nu_1) \int_{|\underset{\sim}{R}_j - \underset{\sim}{R}_i| \geq 2a} \langle A_{j\mu_1\nu_1} \rangle_{ji}\, B^{\mu_1\nu_1}_{\mu\nu}\, d\underset{\sim}{R}_j\right)\right] \qquad (21)$$

Here, n_0 is the number density of the SiC particles.

Equation (21) has the same form as derived in (2) for a distribution of spherical particles. It contains the conditional expectations with two particles held fixed. An approximation to $\langle A_{i\mu\nu} \rangle_i$ is obtained by assuming the Lax (23) quasi-crystalline approximation. This approximation assumes that

$$\langle A_{j\mu_1\nu_1} \rangle_{ji} = \langle A_{j\mu_1\nu_1} \rangle_j \qquad (22)$$

Substitution of Eq. (22) into Eq. (21) leads to an integral equation for the determination of $\langle A_{i\mu\nu} \rangle_i$. To find the effective wave speeds of plane-wave propagation, we assume a solution to the integral equation:

$$\langle A_{i\mu\nu} \rangle_i = X_{\mu\nu}\, e^{iK\zeta_i} \qquad (23)$$

where K is the effective wavenumber and $X_{\mu\nu}$ are constants.

Substituting Eq. (23) into Eq. (21) it can be shown following (2) that for plane-longitudinal and plane-shear waves the respective wavenumbers K_1 and K_2 are

$$\frac{K_1^2}{k_1^2} = \frac{(1+9\bar{c}P_1)\,(1+3\bar{c}P_0)\,(1 + \frac{3}{2}\bar{c}P_2\,(2+3k_2^2/k_1^2))}{1-15\bar{c}P_2\,(1+3\bar{c}P_0) + \frac{3}{2}\bar{c}P_2\,(2+3k_2^2/k_1^2)} \qquad (24)$$

$$\frac{K_2^2}{k_2^2} = \frac{(1+9\bar{c}P_1)\,(1 + \frac{3}{2}\bar{c}P_2\,(2+3k_2^2/k_1^2))}{1 + \frac{3}{4}\bar{c}P_2\,(4-9k_2^2/k_1^2)} \qquad (25)$$

where

$$\bar{c} = \frac{4}{3}\pi abcn_0.$$

Using the expressions for $T^{\mu_1' 1}_{\mu_1 1}$ (9) it is found that

$$9P_1 = (\rho'/\rho - 1) \tag{26}$$

Now writing

$$K_1 = \omega/c_1^*\ ,\ K_2 = \omega/c_2^*$$

where c_1^*, c_2^* are the effective longitudinal-wave and and shear-wave speeds, the effective Lame constants λ^* and μ^* are obtained from the equations

$$\frac{\lambda+2\mu}{\lambda^*+2\mu^*} = \frac{(1+3\bar{c}P_0)}{1-15\bar{c}P_2}\,\frac{\{1+\frac{3}{2}\bar{c}P_2\,(2+3k_2^2/k_1^2)\}}{(1+3\bar{c}P_0)+\frac{3}{2}\bar{c}P_2(2+3k_2^2/k_1^2)} \tag{27}$$

$$\frac{\mu^*}{\mu} = \frac{1+\frac{3}{2}\bar{c}P_2\,(2+3k_2^2/k_1^2)}{1+\frac{3}{4}\bar{c}P_2\,(4-9k_2^2/k_1^2)} \tag{28}$$

The expressions given above can be simplified by using the expressions for $T^{\mu_1\nu}_{\mu_1\nu}$ in (20). The effective bulk modulus and shear modulus are

$$\frac{k^* - k}{k' - k} = \frac{\frac{1}{3}\bar{c}\,T_{mmnn}}{1-\frac{1}{3}\bar{c}\,\frac{k'-k}{k+\frac{4}{3}\mu}\,T_{mmnn}} \tag{29}$$

and

$$\frac{\mu^* - \mu}{\mu' - \mu} = \frac{\frac{1}{5}\bar{c}\,\mu[T_{ijij} - \frac{1}{3}T_{mmnn}]}{\mu - \frac{2\bar{c}}{75}(\mu'-\mu)(3+\frac{2\mu}{\lambda+2\mu})[T_{ijij}-\frac{1}{3}T_{mmnn}]} \tag{30}$$

The tensor T_{ijkl} has been defined in (9). It is noted that in the low-volume concentration limit these agree with the expressions obtained by Boucher (24).

EFFECTIVE WAVE SPEEDS IN A COMPOSITE OF RANDOM DISTRIBUTION OF ORIENTED ELLIPSOIDS

When the ellipsoids are aligned, effective wave speeds of plane waves can be calculated in the same manner as in the previous section by taking the ensemble average of Eq. (12). However, for propagation in an arbitrary direction the dispersion equation is complicated. The equation simplifies for propagation along the ellipsoidal axes. Results for this particular case are given here. Details of the derivation are omitted.

When an incident plane wave propagates along one of the ellipsoid axes, c-axis say, the XYZ axes can be chosen to be parallel to the ellipsoidal abc-axes. Then

$$T^{\mu_1'\nu_1}_{\mu\nu} = T^{\mu_1'\nu_1}_{\mu\nu} \tag{31}$$

Taking now the ensemble average of Eq. (12) one finds

$$\langle A_{i\mu\nu}\rangle_i = \frac{iv_0c^3}{4\pi c^3}\sum_n\sum_m T^{mn}_{\mu\nu}\,[\frac{1}{i}e^{ik_1\zeta_i}\,i^n$$

$$(2n+1)\delta_{m0} + n_0\sum_{\nu_1}\sum_{\mu_1}\int_{|\underline{R}_j-\underline{R}_i|\geq 2a}\langle A_{j\mu\nu}\rangle_j\,i$$

$$A^{\mu_1\nu_1}_{mn}\,d\underline{R}_j + \delta(\nu)\,\{\frac{1}{i}e^{ik_2\zeta_i}\,i^n\,\frac{2n+1}{2n(n+1)}\,(\delta_{m1} -$$

$$n(n+1)\delta_{m,-1}) + n_0\sum_{\nu_1}\sum_{\mu_1}\Delta(\nu_1)\int_{|\underline{R}_j-\underline{R}_i|\geq 2a}$$

$$\langle A_{j\mu_1\nu_1}\rangle_j i\ \ B^{\mu_1\nu_1}_{mn}\,d\underline{R}_j\}] \tag{32}$$

As before, the quasi-crystalline approximation is made to derive an integral equation for $\langle A_{i\mu\nu}\rangle_i$. Considering now a longitudinal-plane-wave solution of this equation ($\langle A_{i\mu\nu}\rangle_i = X_{\mu\nu}e^{iK_1\zeta_i}$; $\mu = 0$, $\nu = 0, 1, 2$) a set of linear homogeneous equations in X_{00}, X_{01}, and X_{02} is obtained. Keeping only the lowest-order terms in K_1^2/k_1^2 and equating the determinant of the coefficients of X_{00}, X_{01}, and X_{02} to zero one finds

$$\frac{K_1^2}{k_1^2} = (1+3\bar{c}\,T^{00}_{01})\,[(1+\bar{c}\,T^{00}_{00})\,(1+\bar{c}\,T^{02}_{02}\,(1+$$

$$\frac{3}{2}k_2^2/k_1^2)) - \bar{c}^2(1+\frac{3}{2}k_2^2/k_1^2)\,T^{02}_{00}\,T^{00}_{02}]/[1-5\bar{c}$$

$$T^{02}_{02}\,(1+\bar{c}\,T^{00}_{00}) + \bar{c}\,(1+\frac{3}{2}k_2^2/k_1^2)\,T^{02}_{02} + \bar{c}\,\{5\,T^{02}_{00}$$

$$+ T^{00}_{02} + 5\,\bar{c}\,T^{02}_{00}\,T^{00}_{02}\}] \tag{33}$$

For a plane shear wave polarized in the X-direction and propagating along the Z-direction the dispersion equation is obtained by taking

$$\langle A_{i\mu\nu}\rangle_i = X_{\mu\nu}\,e^{ik_2\zeta_i}\ ;\ \mu = -1, 1;\ \nu = 1, 2$$

It is found that

$$\frac{K_2^2}{k_2^2} = \frac{(1+3\bar{c}\,T^{11}_{11})[1+\bar{c}(T^{12}_{12}+6T^{-12}_{12})(1+\frac{3}{2}k_2^2/k_1^2)]}{1-\bar{c}\,(T^{12}_{12}+6\,T^{-12}_{12})\,(\frac{9}{4}k_2^2/k_1^2-1)} \tag{34}$$

It is easily shown that for a shear wave polarized along the Y-axis and propagating along the Z-axis the effective wavenumber K_2 is obtained by replacing

$T^{12}_{12} + 6\,T^{-12}_{12}$ with $T^{12}_{12} - 6T^{-12}_{12}$ in Eq. (34).

The above derivation is for propagation along the Z-axis. Results for propagation along the X-axis and

Y-axis are obtained by cyclic interchange of abc. It is shown easily that the speed of propagation of a shear wave polarized along the X-direction and moving along the Z-direction is the same as that of a shear wave polarized along the Z-direction and moving along the X-direction.

WAVE PROPAGATION IN A FIBER-REINFORCED COMPOSITE

The analysis given above can be modified easily to treat wave propagation in a plane perpendicular to the fibers. Propagation of longitudinal and shear waves polarized and propagating in this plane was considered in (1). Although the treatment there was for isotropic fibers, the extension to transversely isotropic fibers is made easily. This was done in (25). In that study the problem of a shear wave polarized along the fibers and propagating perpendicular to them was also considered.

Taking the Z-axis along the fiber axes and denoting the five independent elastic constants characterizing the fibers as C_{11}, C_{12}, C_{13}, C_{33}, and C_{44}, it was shown (25) for SH-wave propagation that the effective wave number β^* is

$$\frac{\beta^{*2}}{k_2^2} = [1 + \bar{c}\,(\rho'/\rho - 1)]\,\frac{1 - \bar{c}\,(m-1)/(m+1)}{1 + \bar{c}\,(m-1)/(m+1)} \qquad (35)$$

where $m = C_{44}/\mu$, $\beta^* = \omega\sqrt{(\rho^*/\mu_{LT})}$, ρ^* the effective density, and μ_{LT} the effective axial shear modulus.

For propagation of longitudinal and shear waves polarized and propagating in a plane perpendicular to the fibers it was found that the corresponding wavenumbers are

$$\frac{K_1^2}{k_1^2} = \frac{\rho^*\,(1 + \bar{c}\,P_o)[1 + \bar{c}\,P_2(1+k_2^2/k_1^2)]}{\rho[1 - \bar{c}\,P_2(1-k_2^2/k_1^2) - 2\bar{c}\,P_oP_2]} \qquad (36)$$

$$\frac{K_2^2}{k_2^2} = \frac{\rho^*/\rho}{1 + \dfrac{2\bar{c}\,(C_{66} - \mu)(\lambda+2\mu)}{2\mu(\lambda+2\mu) + (1-\bar{c})(\lambda+3\mu)(C_{66}-\mu)}} \qquad (37)$$

where

$$P_o = -\frac{K_T' - (\lambda+\mu)}{K_T' + \mu}\,, \quad P_2 = -\frac{\mu(C_{66}-\mu)}{C_{66}(\lambda+3\mu) + \mu(\lambda+\mu)}$$

K_T' is the plane-strain bulk modulus of the fiber

Although the above derivation is for transversely isotropic fibers in an isotropic matrix, it is easily generalized to the case of isotropic fibers in a transversely isotropic matrix with the symmetry axes parallel to the fibers. This is needed to deal with the situation shown in Fig. 2. As in the case of the inclusion problem described above, it is necessary first to calculate the moduli of the effective transversely isotropic composite medium formed by a random homogeneous distribution of fibers in a homogeneous isotropic matrix. In the second step we introduced a distribution of homogeneous isotropic matrix "fibers" into the composite constructed in the first step.

EXPERIMENT

Silicon-Carbide/Aluminum

The photomicrograph shown in Fig. 1 represents an SiC-reinforced Al composite. The material was obtained from a commercial supplier in the form of 1-cm plates. Nominally, the plate contained 30 volume percent SiC.

Sound velocities were determined by a pulse-echo method described in detail previously (15). Briefly, 1-cm cubes were prepared by grinding so that opposite faces were flat and parallel within 5 μm. Quartz piezoelectric crystals with fundamental resonances between 4 and 7 MHz were cemented with phenyl salicylate to the specimens. An x-cut transducer was used for longitudinal waves and an ac-cut for transverse waves. Ultrasonic pulses 1 to 2 cycles long were launched into the specimen by electrically exciting the transducer. The pulses propagated through the specimen, reflected from the opposite face, and propagated back and forth. The pulse echoes were detected by the transducer and displayed on an oscilloscope equipped with a time delay and a microprocessor for time-interval measurements. The sound velocity was computed by

$$v = 2\ell/t$$

where ℓ denotes specimen length, and t the round-trip transit time. On the oscilloscope, t was the time between adjacent echoes, the first and second echoes usually being measured, and within these the time between leading cycles. Elastic constants were computed from the general relationship

$$C = \rho v^2$$

where ρ denotes mass density.

Mass density was determined by Archimedes's method using distilled water as a standard. For 30 volume-percent SiC/Al, we found $\rho = 2.838$ g/cm^3.

Using quantitative-metallographic equipment we verified the overall SiC volume fraction to be $\bar{c} = 28.1 \pm 1.9$ percent and the Al-island concentration to be $c^* = 48.5$ percent. This means that within the sea the SiC volume fraction was 54.6 percent. For the calculations reported below, we took $\bar{c} = 0.30$ and varied c^* from 0.0 to 0.5. Metallography showed that the SiC particles represented as prolate spheroids possess an asepct ratio of approximately 3.0. Similarly, the aluminum islands represented as oblate spheroids possess an aspect ratio of approximately 0.33.

Sapphire (Al_2O_3)/Aluminum and Boron/Aluminum

Figure 2 shows the microstructure of sapphire fiber-reinforced aluminum material, which was obtained from a commerical supplier as 6-mm plates. The matrix consists of a 2%Li-Al alloy. The fibers, 55% by volume, consist of 99+% α-alumina, 20+5 μm diameter, with a manufacturer-reported mass density of 3.95 g/cm^3. Sound velocities, volume fraction, and mass density of the composite were determined as described above for SiC/Al.

Elastic constants of the fiber were estimated from Tefft's (26) monocrystal trigonal-symmetry elastic constants. These were averaged to the quasi-isotropic polycrystal case by a Voigt-Reuss-Hill arithmetic average. The polycrystalline values were then scaled downward slightly to agree with the observed S_{33}, the reciprocal Young's modulus along the fiber direction. For this scaling down, Poisson's ratio was kept fixed.

This gave a fiber Young's modulus of 358 GPa, within the 340-380 GPa range specified by the fiber manufacturer. This estimate assumes isotropic elastic properties in the fiber. In addition to the pulse-echo method we also used the resonance method with a three-component (Marx) oscillator to measure the elastic properties of Boron-Aluminum composite. The details of this can be found in (27).

Creep-Cavities in Copper

Ultrasonic pulse-echo method was used to measure longitudinal sound-wave velocities along and perpendicular to the axis of stress applied to produce creep in polycrystalline copper. The creep cavitation produced is shown in Fig. 3.

RESULTS: CALCULATIONS AND OBSERVATIONS

Effective Elastic Properties

For SiC/Al, Table 1 shows the principal results of the study represented as elastic-stiffness coefficients, C_{ij} in Voigt's notation. Columns 2 and 3 give the properties of the constituents: aluminum alloy 6061 (measured in this study) and SiC (reported by Schreiber and Soga (26)). Column 4 contains the observed elastic constants of 30-volume-percent SiC/Al. Column 6 gives the prediction based on the assumption of homogeneously distributed SiC particles. Finally, column 7 gives predictions based on the present model for the nonhomogeneous case shown in Fig. 1. The co-ordinate system is x_3 perpendicular to plate, x_1 in plate in rolling direction, x_2 in plate perpendicular to rolling direction.

Table 2 - Observed and Predicted Static Elastic Stiffness, C_{ij}, of 55-volume-percent Sapphire-Fiber/Aluminum at Ambient Temperature.

	Al	Sapphire	Obs.	Homog.	Nonhomog.
Spec. grav.	2.706	3.95	3.22	3.39	3.39
C_{11}	1.094	4.193	1.92	1.971	1.985
C_{12}	0.560	1.273	0.66	0.855	0.857
C_{13}	0.560	1.273	0.67	0.780	0.782
C_{33}	1.094	4.193	2.65	2.730	2.730
C_{44}	0.267	1.46	0.64	0.593	0.603
C_{66}	0.267	1.46	0.61	0.558	0.564

Predictions in this table are based on $\bar{c} = 0.55$ and $c^* = 0.10$. Units are $10^{11} N/m^2$.

Table 2 gives similar results for the Al_2O_3/Al fiber-reinforced composite. The co-ordinate system is x_3 in fiber direction. For comparison with theory, we "forced" a transverse-isotropic symmetry on the observations by the relationships $C_{11} = (C_{11} + C_{22})_{obs.}/2$, $C_{13} = (C_{13} + C_{23})_{obs.}/2$, $C_{44} = (C_{44} + C_{55})_{obs.}/2$ and $C_{66} = (2C_{66} + C_{11} - C_{12})_{obs.}/4$.

Table 1 - Observed and Predicted Elastic Stiffnesses, C_{ij}, of 30-Volume-Percent SiC/6061 Al at Room Temperature.

	6061	SiC[a]	30-volume-percent SiC/6061 Al			
			Obs.	R-o-m	Homog.	Nonhomog.
Spec. Grav.	2.706	3.181	2.838	2.849	2.849	2.849
C_{11}	1.105	4.742	1.659	2.195	1.583	1.727
C_{22}	1.105	4.742	1.651	2.195	1.583	1.727
C_{33}	1.105	4.742	1.483	2.195	1.583	1.480
C_{44}	0.267	1.881	0.433	0.751	0.443	0.429
C_{55}	0.267	1.881	0.487	0.751	0.443	0.429
C_{66}	0.267	1.881	0.487	0.751	0.443	0.513
C_{12}	0.571	0.980	0.685	0.693	0.697	0.701
C_{13}	0.571	0.980	0.662	0.693	0.697	0.677
C_{23}[b]	0.571	0.980	0.662	0.693	0.697	0.677[c]

[a] From Schreiber and Soga (28).

[b] We assume $C_{23} = C_{13}$.

[c] We assume $C_{13} = C_{23} = 0.966\ C_{12}$.

Predictions in this table are based on $\bar{c} = 0.30$, $c^* = 0.50$, SiC-particle aspect ratio = 3.0, Al-island aspect ratio = 0.33. Units on C_{ij} are $10^{11} N/m^2$.

For a fiber-reinforced Boron-Aluminum results of observation and predictions of the random-distribution model used in (1) and two other periodic distribution models are shown in Table 3. In the model calculations both constituents were assumed to be isotropic. For the Aluminum matrix this assumption was verified experimentally. However, for Boron fibers the elastic constants are less certain, a wide range of values being reported in the literature. The values shown in Table 3 arose from fitting a linear rule-of-mixtures to our observed S_{33} value combined with Gschneider's (29) recommended values of Boron's bulk modulus. It may be noted that one can derive the properties of Boron by using the observed values and the predictions of the random distribution model. If that is done then it is found that Boron fibers are slightly anisotropic with the properties (all in units of $10^{11}N/m^2$):

$$k_T = 2.693,\ \mu_{LT} = 1.891,\ \mu_{TT} = 2.014$$

$$E_L = 3.72,\ \nu_{LT} = 0.13,\ \nu_T = 0.121,\ E_T = 4.515$$

Table 3 - Observed and Predicted Static Elastic Properties of 48% Boron Fiber/Aluminum Composite at Ambient Temperature

	At	Boron	Observed	Square Model[a]	Hexagonal Model[b]	Random Model[c]	Full Random Model
C_{11}	1.107	4.116	1.852	1.856	1.872	1.790	1.790
C_{12}	0.573	0.590	0.779	-----	0.661	-----	0.745
C_{13}	0.573	0.590	0.606	-----	0.578	-----	0.583
C_{33}	1.107	4.116	2.450	2.480	2.551	-----	2.560
C_{44}	0.267	1.763	0.566	0.451	0.561	0.559	0.559
C_{66}	0.267	1.763	0.526	-----	0.606	0.523	0.523

[a] After Achenbach (30)

[b] After Hlavacek (31)

[c] After (1)

Wave velocities along the c-axis of oriented ellipsoidal inclusions as given by Eqs. (33) and (34) are dependent on the shapes and elastic properties of the ellipsoids. From these one can derive the results for a medium with oriented ellipsoidal shaped cavities. Such is the case depicted in Fig. 3. We show calculated longitudinal wave velocity in the x_3 direction in Fig. 4. It is assumed that the void aspect ratio is 1:10 (c/a). Results for spherical voids are also shown together with the experimentally measured velocities in the x_3 (stress axis) and x_1 directions. This figure shows that the material had some initial anisotropy due to texture which has not been taken into account in the modeling. Assuming completely oriented disc shaped voids one can estimate their aspect ratio by determining which matches the observed curves. For v_3 we obtain 1:7; for v_1 we get 1:12; thus an effective estimate is 1:9. More details of the experiment can be found in (32).

The aspect ratio dependence of elastic velocities in particulate composites as predicted by equations (24) and (25) was studied further in the context of cast iron. Effect of graphite particle shape on Young's modulus of cast iron has been studied experimentally in (33). Similar studies were also reported in (34,35). Fig. 5 shows this dependence using our model. Also shown in this figure are the results of various experimental studies. We made two model calculations corresponding to the properties of graphite by the lower and upper bounds (36). As seen from this figure lower bound properties of graphite give results closer to the experimental observations.

Attenuation

In this section we derive expressions for the attenuation coefficients in a medium containing a distribution of spherical inclusions with thin interface layers through which the elastic properties vary rapidly from those of of the inclusions to those of the matrix. Such interface layers are often present due to processing (see for example (37,38)).

Consider a distribution of spherical inclusions of elastic properties λ_1, μ_1, and density ρ_1 embedded in a matrix material with properties λ_2, μ_2, and ρ_2. Let each inclusion be separated from the matrix by a uniform thin layer of thickness h (<<a) and variable material properties $\lambda(r)$, $\mu(r)$, and $\rho(r)$. Here r is the distance from the center of the sphere and a is its radius. Because of the symmetry the scattered field due to a single sphere can be calculated in an exact form. For the incident field given by (14) it can be shown that, correct to $O(\epsilon^3)$, the scattered field is given by (3) with

$$A_{i\mu\nu} = i\epsilon^3 [P_\nu \phi_{i\mu\nu} + Q_\nu \chi_{i\mu\nu}]$$

$$B_{i\mu\nu} = i\tau^2\epsilon^3 [R_\nu \phi_{i\mu\nu} + S_\nu \chi_{i\mu\nu}] \quad (38)$$

(no sum over ν)

where

$$P_o = \frac{1}{3} \frac{3\lambda_2 + 2\mu_2 - (3\lambda_1 + 2\mu_1)(1 - \frac{h}{a}\frac{3\lambda_2 + 2\mu_2}{\lambda_1' + 2\mu_1'} K_1)}{4\mu_2 + (3\lambda_1 + 2\mu_1)(1 + 4\frac{h}{a}\frac{\mu_2}{\lambda_1' + 2\mu_1'} K_1)}$$

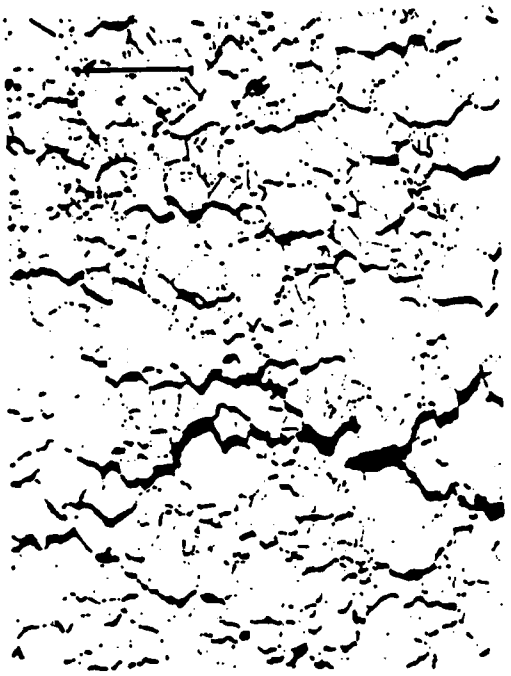

Fig. 3. Photomicrograph of polycrystalline copper containing creep cavities at grain boundaries. Reference mark equals 0.5 mm. Earlier stage shows small disconnected spherical voids.

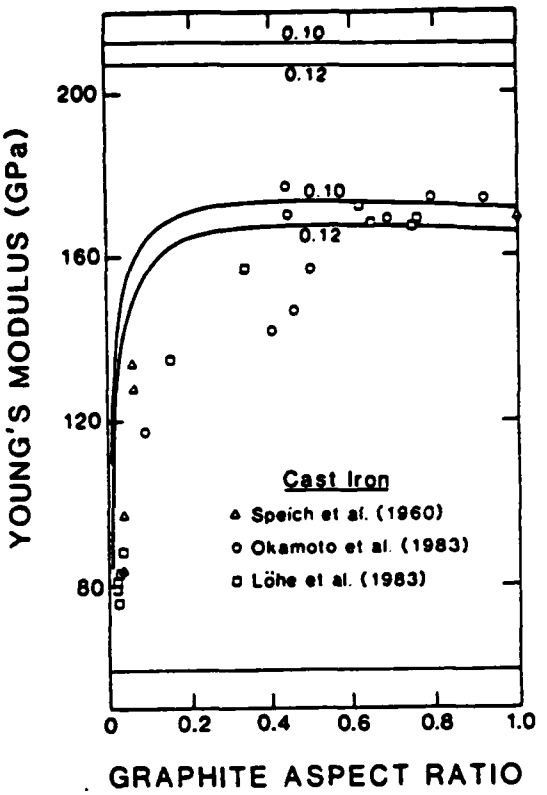

Fig. 5. Variation of Young modulus with graphite-particle aspect ratio. Symbols represent measurements. Curves represent predictions based on present model. Predictions occur for two volume fractions: ten and twelve percent. Upper curves represent upper bounds on graphite's elastic stiffnesses; lower curves represent lower bounds.

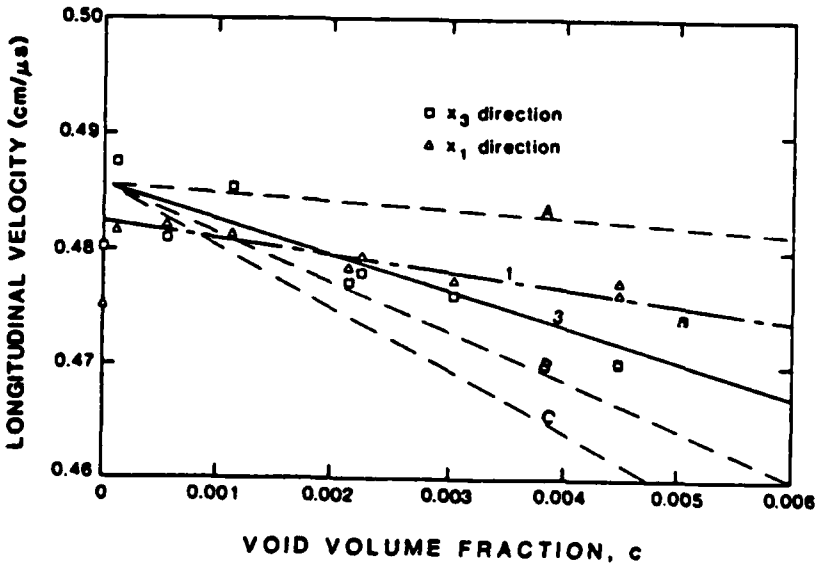

Fig. 4. Longitudinal sound velocity, v, versus volume fraction of voids, c. Lines 1 and 3 represent velocities in directions x_1 and x_3, where x_3 corresponds to the tensile-stress axis and x_1 is perpendicular to x_3. Lines A, B, and C represent calculations: A for spheres, B and C for oblate spheroids (discs) with a 1:10 aspect ratio, where B corresponds to randomly oriented discs and C to discs oriented perpendicular to x_3.

$$Q_0 = R_0 = S_0 = 0$$

$$P_1 = \frac{1}{2\tau} Q_1 = \tau R_1 = S_1 = \frac{1}{9} (\rho_1/\rho_2 - 1)$$

$$P_2 = \frac{1}{3\tau^2} Q_2 = 2R_2 = \frac{2}{3\tau^2} S_2 = \frac{2}{3} (1 - 2\sigma_2) \frac{A}{B}$$

$$A = 1 - \mu_1/\mu_2 + 2 \left(\frac{1}{\alpha} (\mu_1/\mu_2 - \sigma_1) + \frac{h}{a} \frac{1}{\mu_1'} \left(\frac{K_2}{\alpha} + \frac{\mu_1'}{\lambda_1' + 2\mu_1'} K_1 \right)\right)$$

$$B = \frac{\mu_1}{\mu_2} (8 - 10\sigma_2) + 7 - 5\sigma_2 - \frac{1}{\alpha} \left(\frac{\mu_1}{\mu_2} (7 - 11\sigma_2) - 2\sigma_1(5\sigma_2 - 7)\right) - \frac{2h}{a} \frac{\mu_1}{\mu_1'} \left(\frac{K_2}{\alpha} + \frac{\mu_1'}{\lambda_1' + 2\mu_1'} K_1 \right) (5\sigma_2 - 7)$$

$$\frac{1}{\alpha} = [12 \frac{h}{a} \frac{\mu_1}{\mu_1'} (K_2 - \frac{\mu_1'}{\mu_1' + 2\mu_1'} K_1)] / [2(7 - 10\sigma_1) + \frac{\mu_1}{\mu_2} (5 + \sigma_1) + 12 \frac{h}{a} \frac{\mu_1}{\mu_1'} \left(\frac{1}{3} K_2 (7 + 2\sigma_1) + \frac{\mu_1'}{\lambda_1' + 2\mu_1'} K_1 \right)]$$

$$\tau = k_2/k_1 \ , \ c = k_1 a$$

$$\phi_{imn} = (2n + 1) \ i^n \frac{1}{ik_1} \delta_{m0} \ e^{ik_1 \zeta_i}$$

$$X_{imn} = \frac{2n + 1}{n(n + 1)} \ i^n \frac{1}{2ik_2} \{\delta_{m1} - n(n + 1) \ \delta_{m,-1}\} \ e^{ik_2 \zeta_i}$$

$$P_n = Q_n = R_n = S_n = 0 \ , \ n \geq 3$$

In writing the expressions for A_{imn} and B_{imn} we followed the notation of (1) for easy comparison. It was assumed in (1) that $K_1 = 0$ and $K_2 \neq 0$. In the case considered here

$$K_1 = \int_0^1 \frac{dx}{f(a + hx)} \ , \ K_2 = \int_0^1 \frac{dx}{g(a + hx)}$$

where we assumed

$$\lambda(r) + 2\mu(r) = (\lambda_1' + 2\mu_1') \ f(r) \ , \ a \leq r \leq a + h$$

$$\mu(r) = \mu_1' \ g(r) \ , \ a \leq r \leq a + h$$

Following the steps leading to Eqs. (24) and (25) it is then found that the effective wave speeds are given by Eqs. (24) and (25) with the P_ν defined above.

The attenuation caused by scattering can also be calculated by noting that the scattering cross sections for P and S waves are

$$\Sigma_p = \frac{9 v_0 \ c^4}{4\pi a^4} [P_0^2 + 3 (1 + 2\tau^3) \ P_1^2 + 5 (1 + \frac{3}{2} \tau^5) \ P_2^2] \quad (39)$$

$$\Sigma_s = \frac{9 v_0^2 \ c^4 \tau}{4\pi a^4} [3P_1^2 \ (1 + 2\tau^3) + \frac{15}{4} \tau^2 \ P_2^2 \ (1 + \frac{3}{2} \tau^5)] \quad (40)$$

where $v_0 = \frac{4\pi}{3} a^3$. The attenuation coefficients α_p and α_s are then given by

$$\alpha_p = n_0 \Sigma_p \ , \ \alpha_s = n_0 \Sigma_s . \quad (41)$$

Note that attenuation coefficients derived here are for lossless inclusions and matrix. If there is dissipation in either of these materials then there will be additional attenuation which may be derived from (24) and (25) by assuming that λ and μ are complex (see, for example, (40)).

DISCUSSION AND CONCLUSION

A two-step multiple-scattering formalism has been used to predict the anisotropic elastic constants of both particle-reinforced and fiber-reinforced composite materials. Static effective properties are obtained by taking the long-wavelength limit. For both materials, the present model, involving a simple nonhomogeneous distribution of particles or fibers, both explains the elastic anisotropy and gives better absolute predictions of the elastic constants.

In addition we have presented results for phase velocities in a fiber-reinforced material with anisotropic fibers. These indicate that using modeling and observations it is possible to infer the properties of fibers which are sometimes hard to obtain. This aspect of the present study is very useful in other contexts as well, like cast iron with graphite particles.

The modeling reported here is also found to be applicable to medium with oriented or disoriented voids.

Finally, we have presented expressions for attenuation in a medium reinforced by spherical particles with interface layers.

ACKNOWLEDGMENTS

Gratefully, we acknowledge the following essential contributions: DWA Composites Specialties for the SiC/Al material, DuPont for the Al_2O_3/Al material, M.W. Austin for painstaking measurements, Dr. R.J. Fields for quantitative metallography, Dr. R.D. Kriz for computer calculations and graphics, and, finally, DARPA and ONR (Mechanics Division, Grant No. N00014-86-K-0280) for financial support.

REFERENCES

1. Bose, S.K. and Mal, A.K., "Elastic Waves in a Fiber-reinforced Composite," Journal of the Mechanics and Physics of Solids, Vol. 22, 1974, pp. 217-229.

2. Mal, A.K. and Bose, S.K., "Dynamic Moduli of a Suspension of Imperfectly Bonded Spheres," Proceedings of the Cambridge Philosophical Society, Vol. 76, 1974, pp. 587-600.

3. Datta, S.K., "A Self-Consistent Approach to Multiple Scattering of Elastic Waves," Journal of Applied Mechanics, Transactions of ASME, Vol. 44, 1977, pp. 657-662.

4. Devaney, A.J., "Multiple Scattering Theory for Discrete, Elastic, Random Media," Journal of Mathematical Physics, Vol. 21, 1980, pp. 2603-2611.

5. Berryman, J.G., "Long-wavelength Propagation in Composite Elastic Media--I. Spherical Inclusions," Journal of the Acoustical Society of America, Vol. 68, 1980, pp. 1809-1819.

6. Berryman, J.G., "Long-Wavelength Propagation in Composite Elastic Media--II. Ellipsoidal Inclusions," Journal of the Acoustical Society of America, Vol. 68, 1980, pp. 1820-1831.

7. Willis, J.R., "A Polarization Approach to the Scattering of Elastic Waves--II. Multiple Scattering from Inclusions," Journal of the Mechanics and Physics of Solids, Vol. 28, 1980, pp. 307-327.

8. Varadan, V.K., Ma, Y., and Varadan, V.V., "A Multiple Scattering Theory for Elastic Wave Propagation in Discrete Random Media," Journal of the Acoustical Society of America, Vol. 77, 1985, pp. 375-385.

9. Ledbetter, H.M. and Datta, S.K., "Effective Wave Speeds in an SiC-particle-reinforced Al Composite," Journal of the Acoustical Society of America, Vol. 79, 1986, pp. 239-248.

10. Read, D.T. and Ledbetter, H.M., "Elastic Properties of a Boron-Aluminum Composite at Low Temperature," Journal of Applied Physics, Vol. 48, 1977, pp. 2827-2831.

11. Kinra, V.K., Petraitis, M.S., and Datta, S.K., "Ultrasonic Wave Propagation in a Random Particulate Composite," International Journal of Solids and Structures, Vol. 16, 1980, pp. 301-312.

12. Datta, S.K. and Ledbetter, H.M., "Anisotropic Elastic Constants of a Fiber-reinforced Boron-Aluminum Composite," Mechanics of Nondestructive Testing, W.W. Stinchcomb, ed., Plenum Press, New York, 1980, pp. 215-230.

13. Ledbetter, H.M. and Datta, S.K., "Young's Modulus and the Internal Friction of an SiC-particle-reinforced Aluminum Composite," Materials Science and Engineering, Vol. 67, 1984, pp. 25-30.

14. Ledbetter, H.M., "Dynamic Elastic Modulus and Internal Friction in Fibrous Composites," Non-metallic Materials and Composites at Low Temperatures, Plenum Press, New York, 1979, pp. 267-281.

15. Ledbetter, H.M., Frederick, N.V., and Austin, M.W., "Elastic-constant Variability in Stainless Steel," Journal of Applied Physics, Vol. 51, 1980, pp. 305-309.

16. Twersky, V., "Multiple Scattering by Arbitrary Configurations in Three Dimensions," Journal of Mathematical Physics, Vol. 3, 1962, pp. 83-91.

17. Twersky, V., "Multiple Scattering of Electromagnetic Waves by Arbitrary Configurations," Journal of Mathematical Physics, Vol. 8, 1967, pp. 589-610.

18. Datta, S.K., "Diffraction of Plane Elastic Waves by Ellipsoidal Inclusions," Journal of the Acoustical Society of America, Vol. 61, 1977, pp. 1432-1437.

19. Edmonds, A.R., Angular Momentum in Quantum Mechanics, Princeton University Press, New Jersey, 1957.

20. Stein, S., "Addition Theorems for Spherical Wave Functions," Quarterly of Applied Mathematics, Vol. 19, 1961, pp. 15-24.

21. Cruzan, O.R., "Translational Addition Theorems for Spherical Vector Wave Functions," Quarterly of Applied Mathematics, Vol. 20, 1962, pp. 33-40.

22. Hashin, Z. and Shtrikman, S., "A Variational Approach to the Theory of the Elastic Behavior of Multiphase Materials," Journal of the Mechanics and Physics of Solids, Vol. 11, 1963, pp. 127-140.

23. Lax, M. "The Effective Field in Dense Systems," Physical Review, Vol. 88, 1952, pp. 621-629.

24. Boucher, S. "On the Effective Moduli of Isotropic Two-phase Elastic Composites," Journal of Composite Materials, Vol. 8, 1974, pp. 82-89.

25. Datta, S.K., Ledbetter, H.M. and Kriz, R.D., "Calculated Elastic Constants of Composites Containing Anisotropic Fibers," International Journal of Solids and Structures, Vol. 20, 1984, pp. 429-438.

26. Tefft, W.E., "Elastic Constants of Synthetic Single Crystal Corundum," Journal of Research of the National Bureau of Standards, Vol. 70A, 1966, pp. 277-280.

27. Datta, S.K. and Ledbetter, H.M., "Elastic Constants of Fiber-reinforced Boron-Aluminum: Observation and Theory," International Journal of Solids and Structures, Vol. 19, 1983, pp. 885-894.

28. Schreiber, E. and Soga, N., "Elastic Constants of Silicon Carbide," Journal of American Ceramic Society, Vol. 49, 1966, p. 342.

29. Gschneider, K.A., "Physical Properties and Interrelationships of Metallic and Semimetallic Elements," Solid State Physics, Vol. 16, Academic Press, New York, 1964, pp. 275-426.

30. Achenbach, J.D., "Generalized Continuum Theories for Directionally Reinforced Solids," Archives of Mechanics, Vol. 28, 1976, pp. 257-278.

31. Hlavacek, M., "A Continuum Theory of Fiber-reinforced Composites," International Journal of Solids and Structures, Vol. 11, 1975, pp. 199-211.

32. Ledbetter, H.M., Fields, R.J., and Datta, S.K., "Creep Cavities in Copper: An Ultrasonic-Velocity and Composite-Modeling Study," To be published.

33. Okamoto, T., Kagawa, A., Kiyoshi, K., and Matsumoto, H., "Effects of Graphite Shape on Thermal Conductivity, Electrical Resistivity, Damping Capacity and Young's Modulus of Cast Iron below 500 deg. C," Journal of the Japan Foundrymen's Society, Vol. 55, 1983, pp. 32-36.

34. Speich, G.R., Schowoeble, A.J., and Kapadia, B.M., "Elastic Moduli of Gray and Nodular Cast Iron," Journal of Applied Mechanics, Transactions of ASME, Vol. 47, 1980, pp. 821-826.

35. Löhe, D., Vöhringer, O., and Macheranch, E., "Der Einfluß der Graphitform auf den Elastizitätsmodul von ferritischen Gußeisen-werkstoffen," Zeitschrift für Metallkunde, Vol. 74, 1983, pp. 265-273.

36. Wawra, H. Gairola, B.K.D., and Kroner, E., "Comparison between Experimental Values and Theoretical Bounds for the Elastic Constants E, G, K and μ of Aggregates of Noncubic Crystallites," Zeitschrift für Metallkunde, Vol. 73, 1982, pp. 69-71.

37. Rhodes, C.G. and Spurling, R.A., "Fiber-matrix Reaction Zone Growth Kinetics in SiC-Reinforced Ti-6AL-4V as Studied by Transmission Electron Microscopy," Recent Advances in Composites in the United States and Japan, J.R. Vinson and M. Taya, eds., ASTM, Philadelphia, 1983, pp. 585-599.

38. Umekawa, S., Lee, C.H., Yamamoto, J., and Wakashima, K., "Effect of Coatings on Interfacial Reaction in Tungsten/Nickel and Tungsten/316L Composites," Recent Advances in Composites in the United States and Japan, J.R. Vinson and M. Taya, eds., ASTM, Philadelphia, 1983, pp. 619-631.

39. Datta, S.K. and Ledbetter, H.M., "Effect of Interface Properties on Wave Propagation in a Medium with Inclusions," Mechanics of Material Interfaces, A.P.S. Selvadurai and G.Z. Voyiadjis, eds., Elsevier Science Publishers, Amsterdam, 1986, pp. 131-142.

40. Chatterjee, A.K., Mal, A.K., Knopoff, L., and Hudson, J.A., "Attenuation of Elastic Waves in a Cracked, Fluid-Saturated Solid," Mathematical Proceedings of the Cambridge Philosophical Society, Vol. 88, pp. 547-561.

END

10-86

DTIC